THE JOURNAL OF IMMUNOLOGY

Differential Migration of Epidermal and Dermal Dendritic Cells during Skin Infection

Liv Eidsmo, Rhys Allan, Irina Caminschi, Nico van Rooijen, William R. Heath and Francis R. Carbone

J Immunol 2009;182;3165-3172
doi:10.4049/jimmunol.0802950
http://www.jimmunol.org/content/182/5/3165

The Journal of Immunology is published twice each month by
The American Association of Immunologists, Inc.,
9650 Rockville Pike, Bethesda, MD 20814-3994.

Print ISSN: 0022-1767 Online ISSN: 1550-6606.

Differential Migration of Epidermal and Dermal Dendritic Cells during Skin Infection[1]

Liv Eidsmo,* Rhys Allan,* Irina Caminschi,† Nico van Rooijen,‡ William R. Heath,[2]*† and Francis R. Carbone[2]*

Dendritic cells (DCs) are extremely heterogeneous, most evident in the skin where a variety of different subsets have been identified in recent years. DCs of healthy skin include a number of distinct populations in the dermal layer as well as the well-characterized Langerhans cells (LCs) of the epidermis. These steady-state populations are augmented during bouts of local inflammation by additional monocyte-derived DCs. In an effort to better understand the distinction between the different subsets, we examined their behavior following skin infection with HSV. LC emigration rapidly followed appearance of virus in the skin and resulted in depopulation of regions in areas surrounding infected nerve endings. A separate DC population was found to accumulate within the dermis under patches of active epidermal infection with at least some derived from blood monocyte precursors. Ag-positive DCs could occasionally be found in these dermal accumulations, although they represented a minority of DCs in these areas. In addition, infected DCs appeared compromised in their trafficking capabilities and were largely absent from the migrating population. On resolution of skin disease, LCs repopulated the reformed epidermis and these were of mixed origin, with around half entering from the circulation and the remainder derived from local progenitors. Overall, our results show a range of migrational complexities between distinct skin DC populations as a consequence of localized infection. *The Journal of Immunology,* **2009, 182: 3165–3172.**

Dendritic cells (DCs)[3] are key players in T cell stimulation. In recent years, it has become increasingly evident that DCs represent a heterogeneous population (1). This is true for both lymphoid (2) and nonlymphoid tissues (3–7), where one can find the presence of multiple DC subpopulations. It is likely that this DC heterogeneity reflects the diversity in DC contribution to T cell priming or tolerance induction. Of the various known DC populations, plasmacytoid DCs are particularly adept at type I IFN production compared with other DCs to such an extent that this may be their predominant function (8), although Ag presentation has also been attributed to this particular population (9). Within the nonplasmacytoid or conventional subsets, mouse CD8 DCs have been credited with unique cross-presentation ability during cytotoxic T cell priming (10, 11). Some reports suggest that this subset may dominate class I-restricted presentation in general (12), although whether this totally precludes other functionalities or whether specific subsets are specialist helper T cell stimulators remains unclear.

Although certain subsets, such as the CD8 DCs, may be involved in selective MHC presentation, there are likely to be other factors that contribute to the observed DC diversity. An obvious candidate is anatomical localization, such as an origin in lymphoid vs nonlymphoid location. Even positional differences within a given tissue may dictate the existence of distinct and nonoverlapping DC populations. The skin contains a number of DC subsets, with clear differences between the DCs found in the outer epidermis (the Langerhans cells (LCs)) and those located within the underlying dermis layer (the dermal DCs) (13). LCs and dermal DCs are known to migrate to different regions of skin draining lymph nodes (14) and they have been shown to derive from distinct precursors, with LC stem cells residing in the skin and dermal precursors originating largely from the circulation (15, 16). A small subset of dermal DCs are also replaced by local radioresistant cells during bone marrow transplantation (17), consistent with further diversity within this skin-derived population. An additional complexity has been revealed with the recent identification of a unique CD103-staining, langerin-positive dermal population that is different from the epidermal LCs traditionally associated with this latter marker (3–5). Finally, inflammation recruits a separate and distinct DC population of monocytic origins (18). These monocyte-derived DCs have been shown to carry Ag to the draining nodes (19) as well as replenish the LCs that are lost as a consequence of the initial migratory stimulus (17).

Although the above DC complexity has been variously defined and studied in steady-state or nonspecific inflammatory settings, a direct correlation of subset migration and replenishment with the progression of infection has often been lacking. Given this, we set out to accurately define the behavior and movement of the different DC populations of the skin in response to the appearance and ultimately clearance of a highly localized infection of this tissue with a skin tropic pathogen, HSV.

*Department of Microbiology and Immunology, University of Melbourne, Melbourne Victoria, Australia; †Division of Immunology, Walter and Eliza Hall Institute of Medical Research, Melbourne, Victoria, Australia; and ‡Department of Molecular Cell Biology, Faculty of Medicine, Vrije Universiteit Medical Center, Amsterdam, The Netherlands

Received for publication September 5, 2008. Accepted for publication January 3, 2009.

The costs of publication of this article were defrayed in part by the payment of page charges. This article must therefore be hereby marked *advertisement* in accordance with 18 U.S.C. Section 1734 solely to indicate this fact.

[1] This work was supported by grants from the National Health and Medical Research Council of Australia and the Howard Hughes Medical Institute. L.E. was supported by a Swedish Research Council Fellowship.

[2] Address correspondence and reprint requests to Dr. Francis Carbone and Dr. William R. Heath, Department of Microbiology and Immunology, University of Melbourne, 3010, Victoria, Australia. E-mail addresses: fcarbone@unimelb.edu.au and wrheath@unimelb.edu.au

[3] Abbreviations used in this paper: DC, dendritic cell; LC, Langerhans cell; TRITC, tetramethylrhodamine isothiocyanate; MHCII, MHC class II; DAPI, 4′,6-diamidino-2-phenylindole.

www.jimmunol.org/cgi/doi/10.4049/jimmunol.0802950

Materials and Methods

Mice

C57BL/6, B6.SJL PtprcaPep3b/BoyJ (B6.Ly5.1), and C57BL/6-Tg(UBC/GFP)30 Scha/7 were obtained from the Department of Microbiology and Immunology (University of Melbourne, Melbourne, Australia). Mice were housed in specific pathogen-free conditions and all experimentation was conducted according to institutional ethical guidelines.

Generation of bone marrow chimeras

Chimeric mice were generated by irradiation of recipient C57BL/6 mice ($CD45.2^+$) with two doses of 550 Gy, 4 h apart. Four hours after treatment, 5×10^6 B6.Ly5.1 ($CD45.1^+$) bone marrow cells were injected i.v. The mice were allowed to recover for 8 wk before use.

HSV infection

The KOS strain of HSV type 1 was propagated and titrated with VERO cells grown in MEM containing 10% FCS. Mice were inoculated with 1×10^6 PFU of HSV-KOS via the flank scarification model of HSV infection as previously described (20). Viral titers in infected skin were determined by standard plaque-forming assays of homogenized skin on VERO cells.

Cytokine analysis in skin homogenates

TNF-α, IFN-γ, and IL-1β were assayed by using a BD Biosciences cytometric bead array flex set for mice.

Tetramethylrhodamine isothiocyanate (TRITC) painting

TRITC (Invitrogen) was prepared in a 10% stock in DMSO and diluted to 1% solution in acetone. Ten microliters was applied along the zoster site 2 days after infection.

Depletion of circulating monocytes by clodronate-loaded liposome treatment

Cl_2MDP (clodronate) was a gift from Roche Diagnostics and incorporated into liposomes as previously described (21). Two hundred microliters of clodronate-containing liposomes were injected i.v. at the day of infection and thereafter at a daily dose of 150 μl.

Labeling of $Gr1^{high}$ blood monocytes

$Gr1^{high}$ monocytes were labeled by i.v. injection of 200 μl of 0.5 μm of FITC-conjugated microspheres (0.1% solids (w/v) diluted in PBS; Polysciences) in the lateral tail vein 16–18 h after a single dose of 200 μl of clodronate-containing liposomes (18).

HSV infection of bone marrow-derived DCs

Bone marrow collected from C57BL/6-GFP was matured in the presence of GM-CSF (1 μg/ml) and IL-4 (0.3 ng/ml) for 6 days followed by an 18-h maturation in LPS (1 μg/ml) in RPMI 1640 containing 10% FCS and streptomycin. HSV was added in PBS at 5 multiplicity of infection for 1 h before injection. In brief, 3×10^6 cells were injected s.c. in the footpad. Popliteal lymph nodes were harvested 24 h after injection for FACS analysis.

Immunofluorescence microscopy

Skin tissues or lymph nodes were frozen immediately after euthanatization in Tissue-Tek OCT (Sakura Finetek). Sections (8–12 μm) were cut in a cryomicrotome (CM3050S; Leica), air dried, and fixed in ice-cold acetone or 3% paraformaldehyde (CD45.1). Epidermal sheets were prepared as previously described (15). The following primary Abs were used in PBS containing 5% donkey serum (The Jackson Laboratory): rat-anti-langerin (1/500, clone 929F3; Dendritics), polyclonal-rabbit-anti-HSV (1/10, DakoCytomation), biotinylated hamster-anti-CD11c (1/100, clone HL3; BD Biosciences), rat-anti-MHC class II (MHCII; 1/500, clone M5/114), biotinylated rat-anti-FIRE (1/100, clone 6F12, obtained from K. Shortman (22)), rabbit-anti-PGP9.5 (1/500; AbD Serotec), mouse-anti-CD45.1 (1/300; eBioscience), F4/80 (1/400, clone CLA3-1; Caltag Laboratories), and MOMA-1 (1/100, obtained from K. Shortman, The Walter and Eliza Hall Institute, Melbourne, Australia), IL-1b (1/100; R&D Systems). Isotype controls were obtained from BD Biosciences and eBioscience and used at the same concentrations as the primary Abs in combination with secondary reagents. The sections were incubated with primary Abs at 4°C for 16–18 h, followed by incubated for 20 min with secondary Abs at room temperature (streptavidin-Alexa Fluor 488 or 594 and anti-rabbit Alexa Fluor 488, anti-rat Alexa Fluor 594 or 647 (1/750; Molecular Probes).

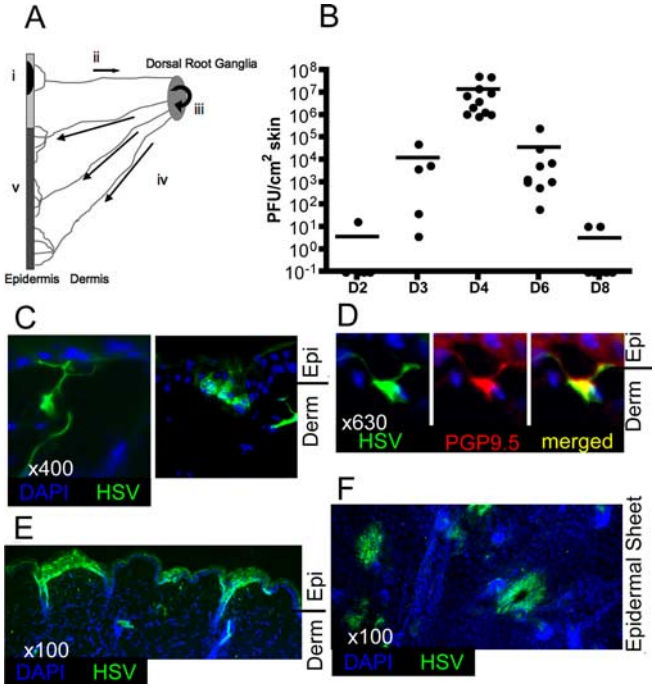

FIGURE 1. Progression of HSV from nerves to skin. *A*, Schematic of the spread of HSV in the zosteriform model of flank infection that shows the primary infection (*i*), the entry of virus into sensory nerve endings and movement to the sensory dorsal root ganglia via retroaxonal flow (*ii*), the second round of virus replication within the ganglia and spread to new nerve bodies (*iii*), the movement of virus in a centrifugal fashion from the dorsal root ganglion (*iv*), and the emergence of virus at a site spatially distinct from the origin of primary inoculation (the zoster site) (*v*). *B*, Viral load at the zoster site of infection between days 2 and 8 after inoculation. *C*, Staining of HSV Ag at day 3 after inoculation at the zoster site in cryosections using anti-HSV Ab (green) and DAPI (blue). *D*, Costaining of nerve endings at the epidermal-dermal junction in infected skin at day 3 after inoculation with anti-PGP9.5 (red) followed by anti-HSV Ab (green). *E*, Patches of infected keratinocytes within the epidermis at the zoster site of infection visualized using anti-HSV Ab (green) and DAPI (blue) in transverse sections and *F*, from above, in epidermal sheets at day 4 after infection.

The staining of PGP9.5 and HSV-1 was performed with anti-PGP9.5 as a primary Ab followed by anti-rat Alexa Fluor 594 and then FITC-conjugated polyclonal anti-HSV-1. FIRE and MHCII were costained by using rat anti-MHCII as a primary Ab, followed by donkey anti-rat-Alexa Fluor 594, then biotinylated anti-FIRE and SAV-Alexa Fluor 488. Slides were mounted with Vectashield containing 4′,6-diamidino-2-phenylindole (DAPI; Vector Laboratories).

All immunostaining was performed in duplicates and repeated at least four times. The density of LCs in epidermis and $langerin^+$ cells in dermis was assessed by counting 10 representative fields per sample at $\times$1000 magnification. Images were acquired using a fluorescence microscope (DMI 4000B; Leica) and digital Leica cameras (models DFC 350 FX and DFC 490; Leica) and were analyzed using IM50 software and Adobe Photoshop. Confocal images were obtained using a Meta 5110 (Leica) and analyzed using Image J or (confocal software). Statistical analysis was performed with Prism 4.0 (Applied Biosystems) using the Mann-Whitney *U* test.

Preparation of single-cell suspension from flank skin tissue

Euthanized mice were perfused with HBSS and a 1-cm^2 piece of skin was removed. Full-thickness skin or epidermal sheets (prepared as previously described (16)) were cut into small pieces and digested for 90 min at 37°C in a solution of RPMI 1640 plus 5 μg/ml DNase I (Sigma-Aldrich) and 3 mg/ml collagenase type III (Sigma-Aldrich) containing 2% FCS. The cell suspensions were passed over 70-μm filter mesh and washed before immunolabeling.

DC isolation from lymph nodes

Popliteal lymph nodes were cut into small fragments and digested at room temperature in RPMI 1640-FCS medium containing collagenase (1 mg/ml,

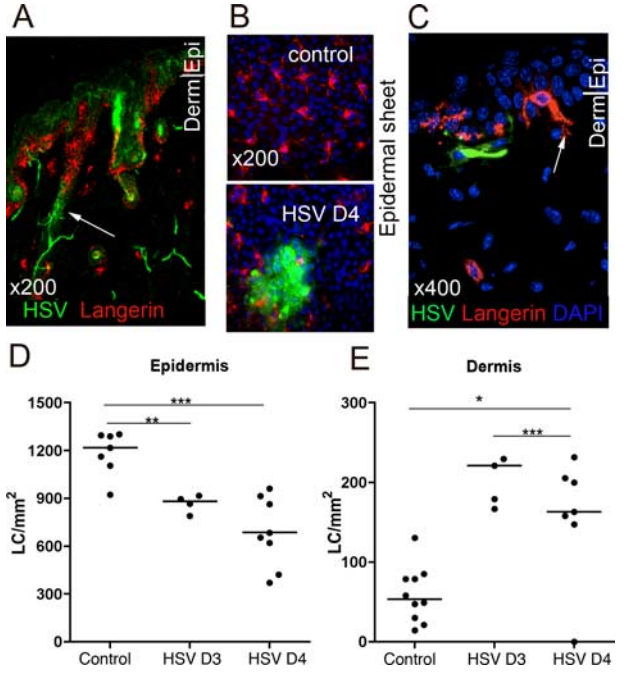

FIGURE 2. Rapid LC emigration on HSV emergence into the skin epidermis. *A*, Transverse section of skin 3 days after infection show costaining of langerin (red) adjacent to a HSV-1 Ag-expressing nerve ending (green, white arrow marks region of interest). *B*, The network of LCs (red) in control epidermal sheets (*upper panel*) and HSV-infected (green) epidermis at day 3 (*lower panel*) with nuclear DAPI staining (blue). *C*, LCs (red) emigrating from the epidermis next to a HSV^+ nerve (green, white arrow). *D*, Dot plots showing density of LCs in epidermis *(right panel)* and dermis (*E*; *left panel*). Median is shown with a horizontal bar (*, $p < 0.05$; **, $p < 0.01$; and ***, $p < 0.001$).

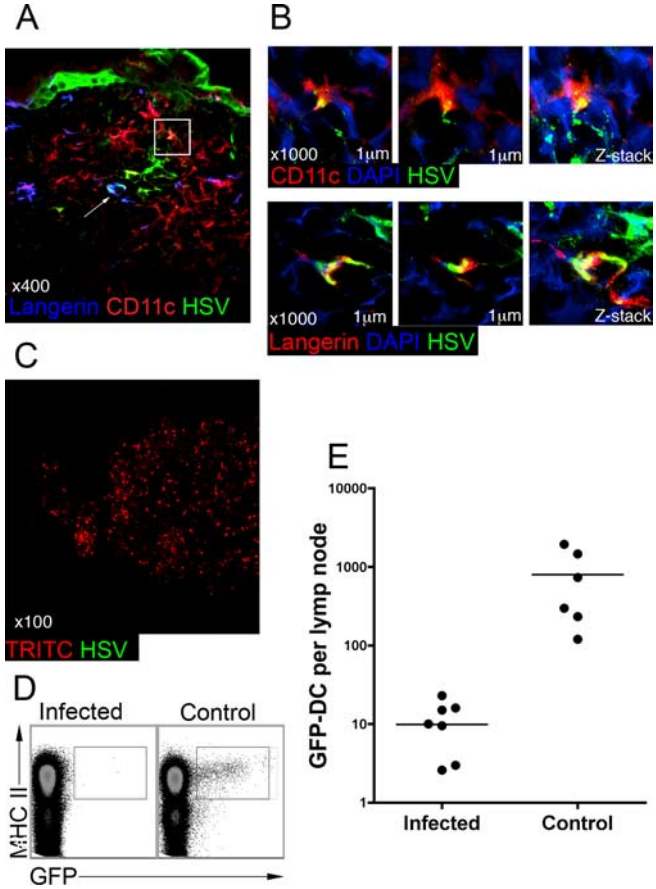

FIGURE 3. Emigration is biased toward noninfected skin DCs. *A*, HSV Ag-positive (green) $CD11c^+$ (solid square) and $langerin^+$ cells (white arrow) in dermis underlying HSV-1-infected epidermis. *B*, *Left* and *middle panel*, 1-μm-thick sections of a HSV^+ (green) $CD11c^+$ (red) cell (*upper panel*) and a HSV^+ (green) $Langerin^+$ (red) cell (*lower panel*). Nuclei were visualized by DAPI (blue). *Right panel*, Z-stack of 12 slices was projected according to maximal intensity. *C*, Costaining of TRITC (red) and HSV (green) in cross-section through a skin draining lymph node 4 days after HSV infection and 48 h after TRITC application to HSV- infected skin. *D*, Representative density plots show live GFP expressing HSV-infected (*left panel*) or control (*right panel*) monocyte-derived DCs in skin draining lymph nodes 24 h after s.c. injection. *E*, Dot plot showing the number of DCs migrated to skin draining lymph nodes. Pooled data from two separate experiments is shown. Mann-Whitney *U* test was used for statistics.

type II; Worthington Biochemical) and DNase I (Boehringer Mannheim) followed by EDTA (1 ml, 0.1 M (pH 7.2)) incubation as previously described (23). DC enrichment was performed by incubation on ice for 30 min with the following mAb: anti-CD3 (KT3-1.1); anti-Thy 1 (T24/31.7, a pan-Thy 1); anti-Gr1 (RB68C5); and anti-erythrocyte (TER-119) followed by incubation with anti-rat Ig-coupled magnetic beads (Dynal). Upon removal of magnetic beads, the DC-enriched fraction was immunolabeled for flow cytometry analysis.

Immunolabeling of single-cell suspensions and flow cytometry

Single-cell suspensions were incubated with an anti-FcIIIR/IIR (clone 2.4G2; BD Pharmingen) mAb in PBS containing 1% BSA. The following Abs were used for immunolabeling: Gr1-allophycocyanin, CD11b-PE-Cy7, MHCII biotinylated, CD45.2-FITC, streptavidine-allophycocyanin-Cy7 (BD Pharmingen), CD45.1-allophycocyanin, and CD11c-Alexa Fluor 700 (eBioscience). The total number of DCs was calculated by adding 2×10^4 BD Pharmingen Sphero Blank calibration particles to each sample and collecting 1×10^4 beads during analysis. The data were collected and analyzed using a FACSCanto II flow cytometer (BD Biosciences) and FlowJo software (Tree Star).

Results

Progression of HSV from nerves to skin during flank zosteriform spread

Flank infection with HSV results in the progressive movement of virus from the site of inoculation into the sensory nerve endings at the point of inoculation (20, 24). The virus then travels to the nerve cell bodies originating in the dorsal root ganglia (Fig. 1*A*). After local replication within the nerve cell bodies, virus spreads to other neurons within a given ganglion before emerging via anterograde axonal flow. Since the intraganglionic spread brings into play additional nerve projections, the virus ultimately emerges over the whole dermatome in a zosteriform band that extends well beyond the original point of contact. In the experiments used here, virus could first be detected at the zoster site of infection around day 3 after inoculation, although there was considerable variation in both the timing of emergence and the amount of virus recovered from independent samples (Fig. 1*B*). Fig. 1*C* shows day 3 postinoculation staining for HSV Ag at this secondary region of infection. The anti-HSV antisera clearly lit up structures at the dermal-epidermal junction of the skin that costained with anti-PGP9.5, which is a ubiquitin protein hydrolase and a specific marker for small nerve fibers in peripheral tissues (25) (Fig. 1*D*). In some cases (Fig. 1*C*, *left panel*), there was little spread of infection into the epidermal layer itself, with few Ag-positive keratinocytes near infected nerve endings. In other cases (Fig. 1*C*, *right panel*), virus could be seen spreading to neighboring keratinocytes at this time and we suspect that these examples correspond to a more advanced course of infection and thus higher titer day 3 samples in Fig. 1*B*. Infection spread from focal points in the epidermis around nerves endings to form infected patches completely contained in the epidermis,

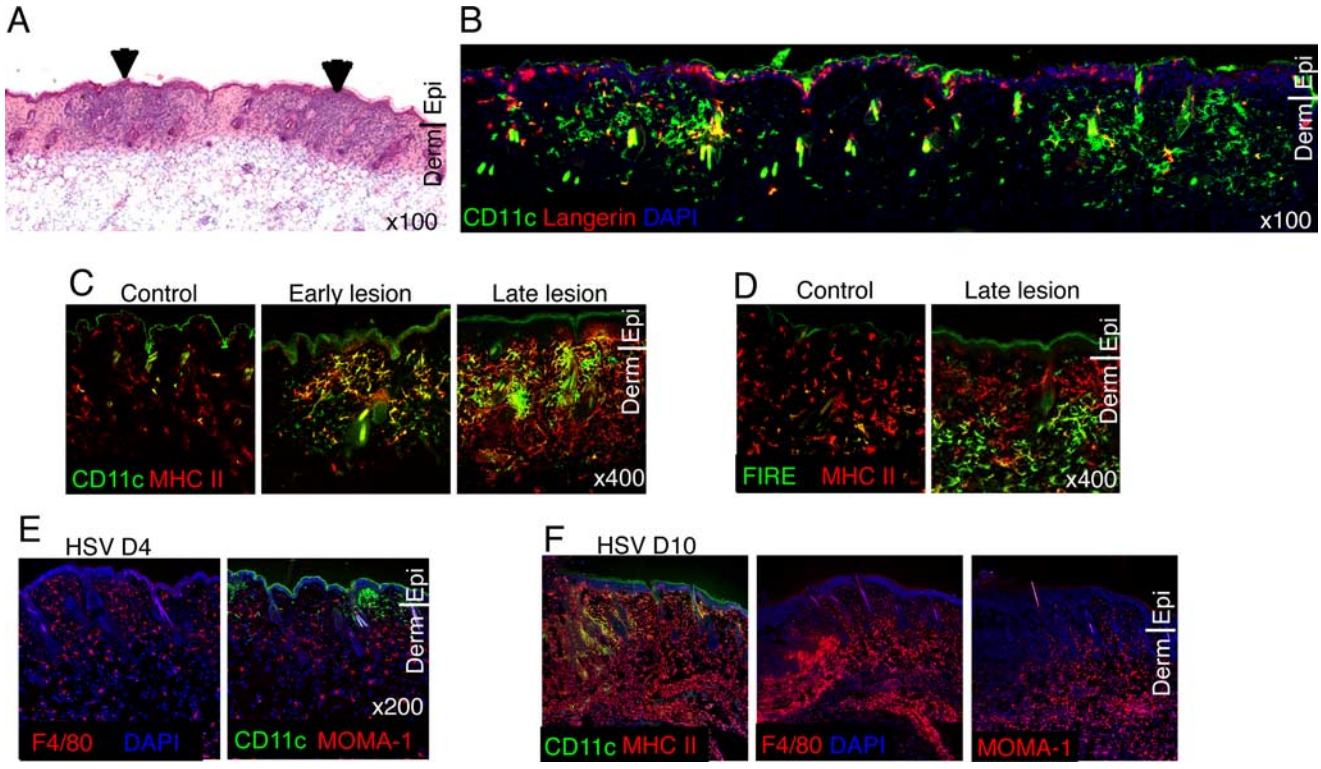

FIGURE 4. Accumulation of DCs in the dermis below areas of HSV infection. *A*, H&E staining 4 days after infection shows focal dermal mononuclear inflammation under two infected epidermal foci (arrowheads). *B*, Costaining of langerin (red) and CD11c (green) in transverse sections of skin 4 days after infection. *C*, Area of scarce (*middle panel*) and dense (*right panel*) inflammation costained for CD11c (green) and MHCII (red) as compared with uninfected skin (*left panel*). *D*, Costaining of FIRE (green) and MHCII (red) in an area of dense inflammation 4 days after infection (*right panel*) as compared with uninfected skin (*left panel*). *E*, Expression of F4/80 (red, *right panel*), MOMA-1 (red), and CD11c (green, *left panel*) in infected skin on day 4. Nuclei were visualized with DAPI (blue). *F*, Expression of CD11c (green), MHCII (red, *left panel*), F4/80 (red, *middle panel*), and MOMA1 (red, *left panel*) counterstained with DAPI (blue) on day 10 after HSV infection.

shown in Fig. 1*E* in transverse sections and Fig. 1*F* as a top view of epidermal sheets.

Rapid LC emigration on HSV emergence into the skin epidermis

Fig. 2*A* shows reduced density of LCs in epidermis within the proximity of emerging virus-positive nerve endings even in the absence of overt infection of neighboring keratinocytes (shown by the arrow), arguing that the arrival of the virus caused rapid LC mobilization and emigration from the skin. This is also evident in the top view of the epidermal sheets shown in Fig. 2*B* (*bottom panel*), which has LC-deficient areas surrounding the infected patches. LCs could also be seen actively leaving the epidermis as shown in Fig. 2*C*. This was also seen in quantitation of skin LC density with time after infection, which revealed a drop in epidermal LC density (Fig. 2*D*) and a corresponding increase in the number of langerin-positive cells in the underlying dermis (Fig. 2*E*), again arguing for virus-induced LC migration from the epidermal layer.

Emigration is biased toward noninfected skin DCs

Given the concomitant emergence of HSV into the epidermal layer and LC emigration in Fig. 2*A*, we looked for the presence of virus-infected LCs within the underlying dermis. Virus-positive DCs were found in this layer (Fig. 3, *A* and *B*), although they were both langerin-positive and negative and thus not exclusively of epidermal origin. In addition, infected cells represented only a minority of all DCs in this region. Thus, it appeared that only a small fraction of emigrating LCs were infected or if infection was widespread, such cells were undergoing rapid elimination. The latter is consistent with the highly cytopathic nature of this virus (26). That infected DCs did not survive migration was suggested by examining TRITC-labeled skin emigrants in the skin draining lymph nodes for signatures of active infection, which showed that the DC migrants were overwhelmingly negative for HSV Ag (Fig. 3*C*). Formal proof that direct DC infection resulted in compromised migration, is shown in Fig. 3, *D* and *E*, where in vitro-infected or control bone marrow-derived DCs were directly injected under the skin to show reduced LN accumulation in the former population. Overall, the results argued that although HSV emergence initiated DC migration from the skin, the cells that entered the lymph node were largely not those infected with virus.

DCs accumulate in the dermis below areas of HSV infection

As the HSV infection spread within the epidermis, areas of dense mononuclear cell infiltrates could be seen within the dermis (Fig. 4*A*). These were directly under the infected epidermal patches (data not shown). Although a few langerin-positive cells were found in these infiltrates, the majority of cells were CD11c positive, langerin negative and thus clearly not of epidermal origin (Fig. 4*B*). Closer examination showed that the dermal accumulation occurred in two waves (Fig. 4*C*), an early wave of moderate cell density under infected surface patches followed by a more extensive accumulation 1 day later as infection spread throughout the epidermis. During the later phase, MHCII-positive but CD11c-negative cells accumulated deep in the dermis under the more superficial $CD11c^+$ infiltrate. This deeper population expressed FIRE, an F4/80-like receptor (Fig. 4*D*), which is found on blood-derived monocytes, tissue macrophages, and a subpopulation of splenic DCs (22). FIRE is down-regulated on the DCs upon stimulation and maturation (22), arguing that this $FIRE^+$ population

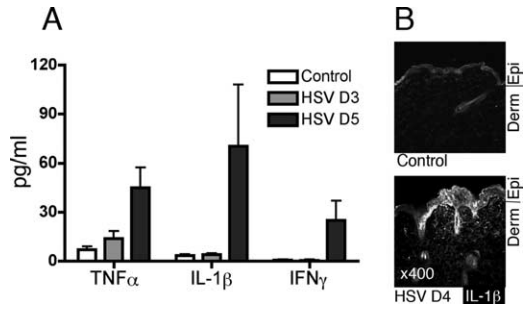

FIGURE 5. Proinflammatory cytokines present at the site of established epidermal HSV infection. *A*, Bar graph showing the concentration of IFN-γ, TNF-α, and IL-1β in skin homogenates from HSV on day 3 (▨), HSV on day 5 (■), and control skin (□). *B*, Expression of IL-1β in healthy skin and HSV-infected skin on day 4.

corresponds to monocytes newly arriving from the circulation. Macrophages were formally identified under accumulating DCs using F4/80, with an even deeper population of MOMA1$^+$ metallophilic macrophages (Fig. 4*E*) similar to what has been reported previously by Dupasquier et al. (27) in healthy skin. MHCII- and F4/80-expressing macrophages were present in high numbers throughout the dermis after disease resolution, whereas MOMA-1-expressing macrophages consistently were found in the deeper parts of the dermis (Fig. 4*F*). These regions represented areas of local inflammation confirmed by up-regulation of TNF-α, IL-1β, and IFN-γ expression in HSV-infected skin (Fig. 5*A*) and the presence of inflammatory cytokines TNF-α (data not shown) and IL-1β around infected areas (Fig. 5*B*), the latter apparently made by the keratinocytes. Furthermore, the levels of the monocyte/macrophage-associated chemokines MIP-1α, MIP-1β, and MCP-1 as well as the keratinocyte-derived chemokine were >10-fold increased in HSV-infected skin as compared with naive skin or HSV-infected skin at the time of virus reemergence (data not shown).

Accumulating DCs are of monocytic origin

Newly infiltrating Gr1$^+$ monocytes recruited into sites of inflammation can be tracked by labeling them with fluorescent beads

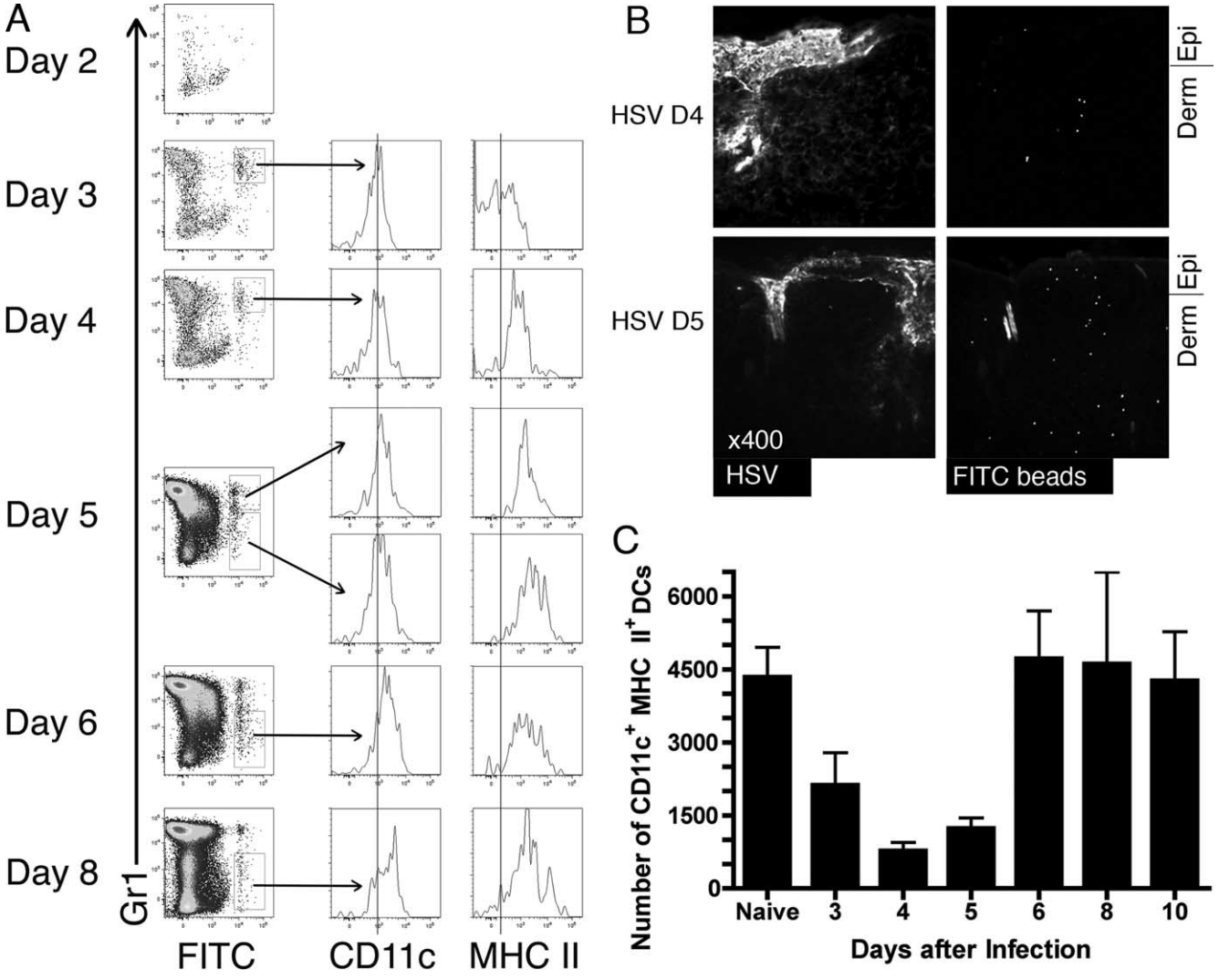

FIGURE 6. DC infiltrates of monocytic origins accumulate in the dermis below areas of HSV infection. *A*, Density plots (*left panel*) showing Gr1 expression combined with FITC-labeled bead content of CD45$^+$ cells from zoster site skin at different times after infection. Histograms (*middle* and *right panels*) show CD11c and MHCII expression of the indicated populations of FITC$^+$Gr1^{high} or FITC$^+$Gr1^{low} cells. Data are representative of three independent experiments. *B*, Staining of HSV (*left panel*) and FITC beads (*right panel*) on day 4 (*upper panel*) and day 5 (*lower panel*) after infection. *C*, The bar graph represents number of CD45$^+$CD11b$^+$Gr1^{low}CD11c$^+$MHCII$^+$ DCs/cm^2 in the skin during the progression of HSV-1 infection. Data were pooled from three independent experiments.

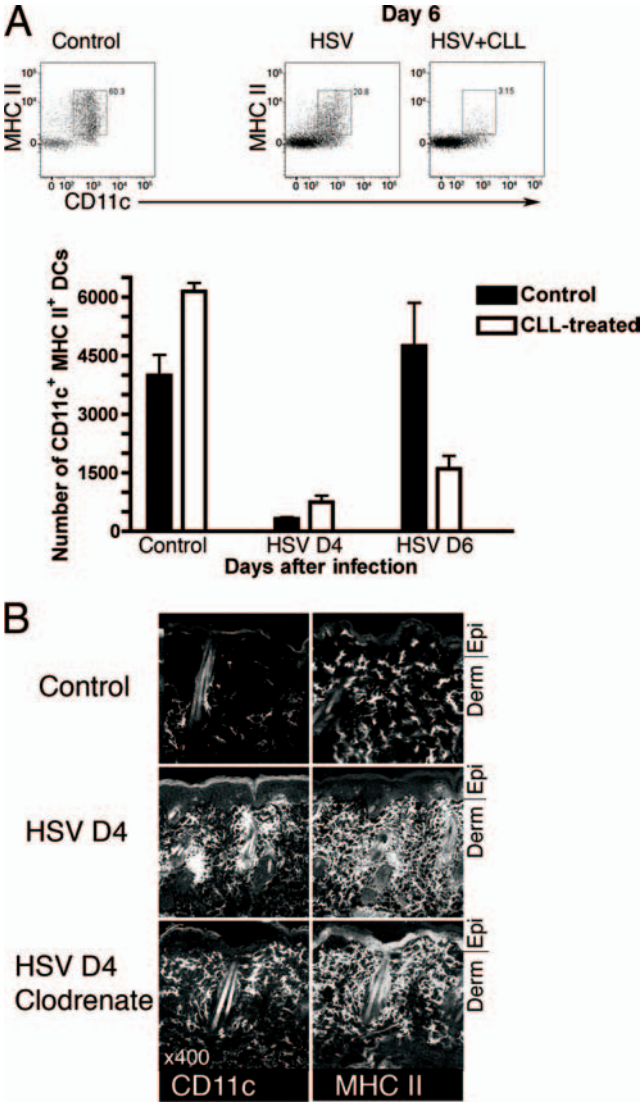

FIGURE 7. Clodronate-loaded liposome (CLL) treatment depletes circulating monocytes and impairs skin DC replenishment during infection. *A*, Representative FACS profiles of $CD45^+CD11c^+MHC\ II^+$ DCs in naive skin and 6 days after infection with or without clodronate treatment (*upper panel*). The bar graph (*lower panel*) shows the number of DCs per cm^2 skin at the times indicated during daily clodronate treatment. Data were pooled from two independent experiments and mean and SE are shown. *B*, Transverse skin sections stained for CD11c (*left panel*) and MHCII (*right panel*) in naive skin (*upper panel*) 4 days after infection (*middle panel*) and 4 days after infection under HSV-infected epidermis after daily clodronate treatment (*lower panel*).

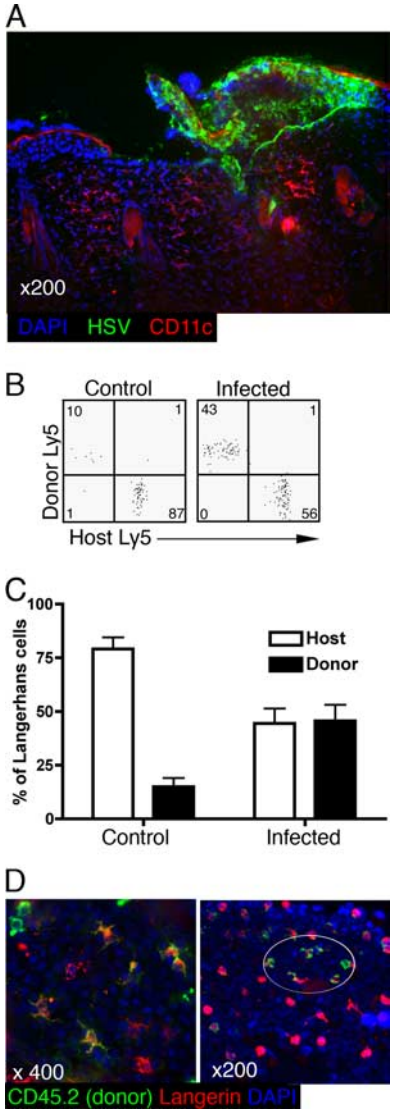

FIGURE 8. On resolution of infection, LC replacement in the reformed epidermis is from mixed local and blood-derived origin. *A*, Transverse section of HSV-infected skin 5 days after infection stained for HSV (green), CD11c (red), and DAPI (blue). The arrow shows shedding of HSV^+ epithelium. *B*, Representative dot plots from epidermal sheets prepared from healthy skin (controls) and scar tissue 30 days after HSV infection (infected) stained for Ly5.1 and Ly5.2. *C*, Bar graphs show the origin of epidermal $CD11c^+MHCII^+$ cells in CD45.1 (donor)→CD45.2 (host) bone marrow chimeric mice 1 mo after HSV-1 infection assessed by FACS. Mean and SE from data pooled from two independent experiments are shown. *D*, Epidermal sheets covering HSV- induced scar tissue stained for CD45.1 (green) and langerin (red) 1 mo after HSV infection with clusters of donor-derived cells shown *circled* in the *right panel*.

after transient elimination of the $Gr1^-$ population of circulating monocytes using clodronate-loaded liposomes (18). Fig. 6*A* shows the infiltration of a $Gr1^+FITC^+$ subset into skin around 2 days after infection as detected by flow cytometric analysis of whole skin. This population was replaced by bead-positive DCs that were $Gr1^-CD11c^+MHCII^+$, starting around day 3 after infection at low numbers and reaching peak levels after day 5. Populations of FITC bead-containing cells were also detected under infected epidermis by histological analysis (Fig. 6*B*). The increase in bead-labeled $CD11c^+$ cells in the skin mirrored the overall increase in total $CD11c^+MHCII^+$ cells from day 6 after infection (Fig. 6*C*). It should be noted that there was a transient loss of cells with these markers, reaching a numerical nadir around day 4 (Fig. 6*C*). This likely reflects emigration of DCs seen after the first arrival of HSV into the skin.

That monocyte-derived DCs accumulated in infected skin was confirmed by showing that clodronate-loaded liposome ablation of circulating monocytes reduced the $CD11c^+MHCII^+$ cells in infected but not naive mice, as detected by flow cytometry (Fig. 7*A*). In addition, this treatment appeared to also reduce the intensity of MHCII and CD11c staining under the infected epidermal patches on day 4 as shown in Fig. 7*B*. Overall, the data argued that at least some of the cells that accumulated under the HSV-infected epidermis were of monocytic origin and that these cells replaced DCs that had left the skin as a consequence of HSV infection.

On resolution of infection, LC replacement in the reformed epidermis is from mixed local and blood-derived origin

The zosteriform disease resulted in considerable damage to the skin and complete destruction of the epidermis (Fig. 8*A*). It has been reported that LCs can be replaced from precursors that originate in the blood, such as those of monocyte origin (17, 28). In addition, LC precursors also exist within the skin itself (15). Given this, we set out to determine whether both cell types could equally repopulate the epidermis that reformed after resolution of infection. To do this, we took advantage of the finding that the local LC precursors survive irradiation (15), whereas the blood-derived population can be replaced by bone marrow reconstitution (16). Fig. 8, *B* and *C*, shows that LCs in the healed epidermis were nearly equally of host and donor origin 1 mo after infection compared with control uninfected mice, where 80% of LCs in control skin where donor derived. The replacement of LCs by both host- and donor-derived precursors was also evident in histological analysis (Fig. 8*D*). Moreover, the histology showed that these cells were interspersed, suggesting a random reconstitution of LCs by distinct precursors (Fig. 8*D*, *left panel*), although clusters could occasionally be seen in the epidermal sheets (Fig. 8*D*, *right panel*). Overall, although destruction of the epidermis resulted in considerable replacement by blood-derived LC precursors, a local population nonetheless made a significant contribution to the replenishment of this tissue.

Discussion

The zosteriform model of HSV infection has unique advantages when it comes to the examination of DC behavior in the skin. The pathogen enters the skin via an endogenous axonal-mediated route and thus does not involve any form of tissue trauma, which is a known stimulus for skin DC migration (29). Separately, virus replication is largely confined to the epidermis, making it a perfect model to study LC behavior in the face of infection in this location. As can be seen in this study, the infection proceeds from nerve endings to adjacent cells in the epidermal layer. Temporal tracking of LC migration showed that they were mobilized very fast after appearance of virus in the skin. Indeed, changes in LC staining could be seen when virus Ags were largely confined to the nerve endings and before extensive infection of the adjacent keratinocytes. It has been shown that LCs are poor contributors to T cell activation after HSV infection (16, 30). A rapid mobilization and emigration from the skin before extensive spread of infection could, in part, explain their lack of presentation. In addition, infected DCs are functionally compromised and rapidly die (26, 31), which would further decrease their contribution to overall T cell priming. Our results reinforced this by showing that few migrants within the draining lymph nodes expressed HSV Ags and that infection with this virus actually inhibited DC migration.

One striking result from this study is the observed difference in behavior of epidermal LCs and the dermal DC populations. The epidermal regions around infection appeared to be largely devoid of LCs, consistent with their rapid emigration from this layer of skin. In contrast, there was a marked accumulation of DCs in the dermis just under infected areas. A similar pattern of subepithelial accumulation was also seen in vaginal infections with HSV-2 (30). In that case it was not determined whether the DCs were all of local origin or whether some had entered from some external source, although a subsequent study suggested that infiltrates were indeed of monocytic origin (32). In this study, the dermal DC accumulations include a monocyte-derived population, determined by a combination of bead tracking and clodronate depletion. The flow cytometric studies showed a conversion of the recruited FITC-bead-positive cells from $Gr1^+CD11c^-$ infiltrating monocytes to a Gr^-CD11c^+ DC population, as reported in other cases of local inflammation (17). Interestingly, histological assessment showed that cells with a monocyte phenotype, marked by expression of FIRE, were located much deeper in the dermis than the $CD11c^+$ DCs. This suggests the existence of some form of maturation gradient toward the dermal-epidermal junction and possibly the migration of monocyte-derived DCs toward the infected epidermis. If so, such migration would be distinct from what was seen with the epidermal LCs, which migrated in the opposite direction on first appearance of pathogen, most likely en route to the lymph nodes.

Skin DC numbers decline with infection, reaching relatively low levels by day 4 after inoculation (Fig. 4*C*). It is likely that the increases seen after this time reflected recruitment of monocytes and their conversion to a dermal DC population. Treatment with clodronate-loaded liposomes significantly reduced the DC content at day 6 after infection, at a time when monocytes were seen converting to a $Gr1^-CD11c^+$ population. This result argued that majority of DCs were of monocytic origin as infection progressed, although we assume that this is not the only means of local DC replenishment. Nonetheless, HSV-induced replacement by monocytes recruited from the circulation is consistent with the results from vaginal infection (32). The newly recruited DCs may be involved in continuous trafficking of Ag to the draining lymph nodes and it has been shown that such DCs can indeed transport skin-derived material in this matter (19). Alternatively, this relatively late DC infiltration may serve another purpose, such as the stimulation of T cells within the infected skin itself. Local DC stimulation has been shown in the case of memory and effector T cell populations (33, 34). In addition, the recruited monocytes could well be the precursors of long-lived DC populations that persist after the resolution of infection. It has been shown that LCs can, in part, be derived from monocytic precursors subsequent to skin inflammation (17). In this study, infection resulted in extensive damage to the outer epithelial layer of the skin, which is reformed by around days 9–10 after inoculation. The LCs that repopulated this reformed skin were found to be of mixed origin, either derived from radioresistant LC precursors or recruited from some radiosensitive subset, presumably derived from the circulation. Both populations were intermixed and were evenly spread in the epidermal layer, which is different to what is seen in other cases of skin and mucosal LC ablation (3, 17, 32). One difference between the situation here and the previous reports, which involved near complete elimination of all LCs, is that the skin surrounding the site of infection was left relatively unaffected. As a consequence, these intact epidermal areas could contribute the local precursors that partly replenish the lost LC population.

Overall, this study shows that the skin DC populations behave in a complex fashion after infection in the skin, both in terms of their migrational characteristics and their localization in the skin. Such results build on the growing evidence that the different DC subsets are indeed unique and distinct in their functional capacities.

Acknowledgments

We thank Dr. Ken Shortman for provision of reagents used in this study.

Disclosures

The authors have no financial conflict of interest.

References

1. Villadangos, J. A., and W. R. Heath. 2005. Life cycle, migration and antigen presenting functions of spleen and lymph node dendritic cells: limitations of the Langerhans cells paradigm. *Semin. Immunol.* 17: 262–272.

2. Shortman, K., and S. H. Naik. 2007. Steady-state and inflammatory dendritic-cell development. *Nat. Rev.* 7: 19–30.
3. Poulin, L. F., S. Henri, B. de Bovis, E. Devilard, A. Kissenpfennig, and B. Malissen. 2007. The dermis contains langerin$^+$ dendritic cells that develop and function independently of epidermal Langerhans cells. *J. Exp. Med.* 204: 3119–3131.
4. Ginhoux, F., M. P. Collin, M. Bogunovic, M. Abel, M. Leboeuf, J. Helft, J. Ochando, A. Kissenpfennig, B. Malissen, M. Grisotto, et al. 2007. Blood-derived dermal langerin$^+$ dendritic cells survey the skin in the steady state. *J. Exp. Med.* 204: 3133–3146.
5. Bursch, L. S., L. Wang, B. Igyarto, A. Kissenpfennig, B. Malissen, D. H. Kaplan, and K. A. Hogquist. 2007. Identification of a novel population of Langerin$^+$ dendritic cells. *J. Exp. Med.* 204: 3147–3156.
6. Iwasaki, A. 2007. Mucosal dendritic cells. *Annu. Rev. Immunol.* 25: 381–418.
7. de Heer, H. J., H. Hammad, M. Kool, and B. N. Lambrecht. 2005. Dendritic cell subsets and immune regulation in the lung. *Semin. Immunol.* 17: 295–303.
8. Siegal, F. P., N. Kadowaki, M. Shodell, P. A. Fitzgerald-Bocarsly, K. Shah, S. Ho, S. Antonenko, and Y. J. Liu. 1999. The nature of the principal type 1 interferon-producing cells in human blood. *Science* 284: 1835–1837.
9. Salio, M., M. J. Palmowski, A. Atzberger, I. F. Hermans, and V. Cerundolo. 2004. CpG-matured murine plasmacytoid dendritic cells are capable of in vivo priming of functional CD8 T cell responses to endogenous but not exogenous antigens. *J. Exp. Med.* 199: 567–579.
10. den Haan, J. M., S. M. Lehar, and M. J. Bevan. 2000. CD8$^+$ but not CD8$^-$ dendritic cells cross-prime cytotoxic T cells in vivo. *J. Exp. Med.* 192: 1685–1696.
11. Pooley, J. L., W. R. Heath, and K. Shortman. 2001. Cutting edge: intravenous soluble antigen is presented to CD4 T cells by CD8 $^-$dendritic cells, but cross-presented to CD8 T cells by CD8$^+$ dendritic cells. *J. Immunol.* 166: 5327–5330.
12. Dudziak, D., A. O. Kamphorst, G. F. Heidkamp, V. R. Buchholz, C. Trumpfheller, S. Yamazaki, C. Cheong, K. Liu, H. W. Lee, C. G. Park, R. M. Steinman, and M. C. Nussenzweig. 2007. Differential antigen processing by dendritic cell subsets in vivo. *Science* 315: 107–111.
13. Valladeau, J., and S. Saeland. 2005. Cutaneous dendritic cells. *Semin. Immunol.* 17: 273–283.
14. Kissenpfennig, A., S. Henri, B. Dubois, C. Laplace-Builhe, P. Perrin, N. Romani, C. H. Tripp, P. Douillard, L. Leserman, D. Kaiserlian, et al. 2005. Dynamics and function of Langerhans cells in vivo: dermal dendritic cells colonize lymph node areas distinct from slower migrating Langerhans cells. *Immunity* 22: 643–654.
15. Merad, M., M. G. Manz, H. Karsunky, A. Wagers, W. Peters, I. Charo, I. L. Weissman, J. G. Cyster, and E. G. Engleman. 2002. Langerhans cells renew in the skin throughout life under steady-state conditions. *Nat. Immunol.* 3: 1135–1141.
16. Allan, R. S., C. M. Smith, G. T. Belz, A. L. van Lint, L. M. Wakim, W. R. Heath, and F. R. Carbone. 2003. Epidermal viral immunity induced by CD8α^+ dendritic cells but not by Langerhans cells. *Science* 301: 1925–1928.
17. Ginhoux, F., F. Tacke, V. Angeli, M. Bogunovic, M. Loubeau, X. M. Dai, E. R. Stanley, G. J. Randolph, and M. Merad. 2006. Langerhans cells arise from monocytes in vivo. *Nat. Immunol.* 7: 265–273.
18. Tacke, F., F. Ginhoux, C. Jakubzick, N. van Rooijen, M. Merad, and G. J. Randolph. 2006. Immature monocytes acquire antigens from other cells in the bone marrow and present them to T cells after maturing in the periphery. *J. Exp. Med.* 203: 583–597.
19. Randolph, G. J., K. Inaba, D. F. Robbiani, R. M. Steinman, and W. A. Muller. 1999. Differentiation of phagocytic monocytes into lymph node dendritic cells in vivo. *Immunity* 11: 753–761.
20. van Lint, A., M. Ayers, A. G. Brooks, R. M. Coles, W. R. Heath, and F. R. Carbone. 2004. Herpes simplex virus-specific CD8$^+$ T cells can clear established lytic infections from skin and nerves and can partially limit the early spread of virus after cutaneous inoculation. *J. Immunol.* 172: 392–397.
21. Van Rooijen, N., and A. Sanders. 1994. Liposome mediated depletion of macrophages: mechanism of action, preparation of liposomes and applications. *J. Immunol. Methods* 174: 83–93.
22. Caminschi, I., K. M. Lucas, M. A. O'Keeffe, H. Hochrein, Y. Laabi, F. Kontgen, A. M. Lew, K. Shortman, and M. D. Wright. 2001. Molecular cloning of F4/80-like-receptor, a seven-span membrane protein expressed differentially by dendritic cell and monocyte-macrophage subpopulations. *J. Immunol.* 167: 3570–3576.
23. Vremec, D., J. Pooley, H. Hochrein, L. Wu, and K. Shortman. 2000. CD4 and CD8 expression by dendritic cell subtypes in mouse thymus and spleen. *J. Immunol.* 164: 2978–2986.
24. Simmons, A., and A. A. Nash. 1984. Zosteriform spread of herpes simplex virus as a model of recrudescence and its use to investigate the role of immune cells in prevention of recurrent disease. *J. Virol.* 52: 816–821.
25. Yamaoka, J., Z. H. Di, W. Sun, and S. Kawana. 2007. Changes in cutaneous sensory nerve fibers induced by skin-scratching in mice. *J. Dermatol. Sci.* 46: 41–51.
26. Jones, C. A., M. Fernandez, K. Herc, L. Bosnjak, M. Miranda-Saksena, R. A. Boadle, and A. Cunningham. 2003. Herpes simplex virus type 2 induces rapid cell death and functional impairment of murine dendritic cells in vitro. *J. Virol.* 77: 11139–11149.
27. Dupasquier, M., P. Stoitzner, A. van Oudenaren, N. Romani, and P. J. Leenen. 2004. Macrophages and dendritic cells constitute a major subpopulation of cells in the mouse dermis. *J. Invest. Dermatol.* 123: 876–879.
28. Holzmann, S., C. H. Tripp, M. Schmuth, K. Janke, F. Koch, S. Saeland, P. Stoitzner, and N. Romani. 2004. A model system using tape stripping for characterization of Langerhans cell-precursors in vivo. *J. Invest. Dermatol.* 122: 1165–1174.
29. Lessard, R. J., K. Wolff, and R. K. Winkelmann. 1968. The disappearance and regeneration of Langerhans cells following epidermal injury. *J. Invest. Dermatol.* 50: 171–179.
30. Zhao, X., E. Deak, K. Soderberg, M. Linehan, D. Spezzano, J. Zhu, D. M. Knipe, and A. Iwasaki. 2003. Vaginal submucosal dendritic cells, but not Langerhans cells, induce protective Th1 responses to herpes simplex virus-2. *J. Exp. Med.* 197: 153–162.
31. Salio, M., M. Cella, M. Suter, and A. Lanzavecchia. 1999. Inhibition of dendritic cell maturation by herpes simplex virus. *Eur. J. Immunol.* 29: 3245–3253.
32. Iijima, N., M. M. Linehan, S. Saeland, and A. Iwasaki. 2007. Vaginal epithelial dendritic cells renew from bone marrow precursors. *Proc. Natl. Acad. Sci. USA* 104: 19061–19066.
33. McGill, J., N. Van Rooijen, and K. L. Legge. 2008. Protective influenza-specific CD8 T cell responses require interactions with dendritic cells in the lungs. *J. Exp. Med.* 205: 1635–1646.
34. Wakim, L. M., J. Waithman, N. van Rooijen, W. R. Heath, and F. R. Carbone. 2008. Dendritic cell-induced memory T cell activation in nonlymphoid tissues. *Science* 319: 198–202.